PNAS RESEARCH ARTICLE | CHEMISTRY

Transient learning degrees of freedom for introducing function in materials

Varda F. Hagh[a,b,1], Sidney R. Nagel[a], Andrea J. Liu[c], M. Lisa Manning[d,e], and Eric I. Corwin[b]

Edited by Robert Connelly, Cornell University, Ithaca, NY; received September 24, 2021; accepted March 8, 2022 by Editorial Board Member Paul Chaikin

The introduction of transient degrees of freedom into a system can lead to novel material design and training protocols that guide a system into a desired metastable state. In this approach, some degrees of freedom, which were not initially included in the system dynamics, are first introduced and subsequently removed from the energy minimization process once the desired state is reached. Using this conceptual framework, we create stable jammed packings that exist in exceptionally deep energy minima marked by the absence of low-frequency quasilocalized modes; this added stability persists in the thermodynamic limit. The inclusion of particle radii as transient degrees of freedom leads to deeper and much more stable minima than does the inclusion of particle stiffnesses. This is because particle radii couple to the jamming transition, whereas stiffnesses do not. Thus, different choices for the added degrees of freedom can lead to very different training outcomes.

metamaterials | material training | jamming | degrees of freedom | mechanical stability

Systems with disorder often have a complex and rugged energy landscape whose minima are determined by the system's degrees of freedom and constraints. Finding low-lying states in such a system is a daunting challenge that lies at the heart of many constraint satisfaction statistical physics problems, ranging from machine learning to population ecology (1–4). More difficult is finding rare minima in such systems that have specific desired properties or functions such as enhanced stability against external perturbations. Finding a framework for designing a desired function into a complex system in a flexible and reliable manner is an important goal that could lead to a paradigm shift in material processing.

There is an unappreciated but common feature of many of the protocols that have recently been proposed to create ground states with special properties. In each case, new "learning" degrees of freedom, not contained in the original description, are added to the system. That is, some constraints are relaxed and allowed to vary according to a set of dynamical rules. These degrees of freedom are then manipulated to produce the desired behavior before being removed. We term these "free-then-freeze" optimization protocols.

To make this explicit, we give a few examples. For the tuning-by-pruning protocol for dilution of bonds in an elastic network (5–9), the new degree of freedom is the possibility of removing a bond. For the directed-aging protocol for evolving function by aging a material under imposed strains (10–12), the new degree of freedom in this case is the evolution of the stiffness or length of each bond. For the swap Monte Carlo protocol for allowing long-ranged exchange of particles with different sizes (13–17), the new degrees of freedom are the particle swaps. More generally, neural networks are tuned by varying node or edge properties to learn tasks.

Introducing new learning degrees of freedom alters the energy landscape and, as some of these protocols have demonstrated, allows states with rare and desired properties to be accessed. Moreover, these degrees of freedom are transient: they are accessible during the system evolution but are subsequently frozen. They can be removed either explicitly (by freezing them after the training has been completed) or implicitly (by noting that a separation of time scales can appear naturally during evolution so that some relaxations are no longer possible). We note that this process is akin to learning in the context of machine learning. Thereby, we can profitably think of these newly introduced variables as learning degrees of freedom.

While similar protocols have been studied in a wide range of networks or thermal systems, here we focus on athermal particulate materials, which have historically proven more difficult to program with specific macroscopic properties and functions. This is because in such systems, states with desired properties must correspond to local minima. Such minima are typically separated by rather low barriers that are surmounted via localized rearrangements that change particle neighbors. This can lead to long-range elastic stresses and reorganization within the material via avalanches, making it difficult to control final properties.

Significance

Many protocols used in material design and training have a common theme: they introduce new degrees of freedom, often by relaxing away existing constraints, and then evolve these degrees of freedom based on a rule that leads the material to a desired state at which point these new degrees of freedom are frozen out. By creating a unifying framework for these protocols, we can now understand that some protocols work better than others because the choice of new degrees of freedom matters. For instance, introducing particle sizes as degrees of freedom to the minimization of a jammed particle packing can lead to a highly stable state, whereas particle stiffnesses do not have nearly the same impact.

Author affiliations: [a]James Franck Institute, University of Chicago, Chicago, IL 60637; [b]Department of Physics and Materials Science Institute, University of Oregon, Eugene, OR 97403; [c]Department of Physics, University of Pennsylvania, Philadelphia, PA 19104; [d]Department of Physics, Syracuse University, Syracuse, NY 13244; and [e]BioInspired Institute, Syracuse University, Syracuse, NY 13244

Author contributions: V.F.H., S.R.N., A.J.L., M.L.M., and E.I.C. designed research; V.F.H. performed research; V.F.H. and E.I.C. contributed new reagents/analytic tools; V.F.H. analyzed data; and V.F.H., S.R.N., A.J.L., M.L.M., and E.I.C. wrote the paper.

The authors declare no competing interest.

This article is a PNAS Direct Submission. R.C. is a Guest Editor invited by the Editorial Board.

[1]To whom correspondence may be addressed. Email: vardahagh@uchicago.edu.

This article contains supporting information online at https://www.pnas.org/lookup/suppl/doi:10.1073/pnas.2117622119/-/DCSupplemental.

Published May 5, 2022.

Jammed particle packings are a paradigmatic category of athermal particulate systems. Jamming here refers to a rigidity transition in which the system becomes rigid due to compression. This occurs at a critical density or packing fraction, ϕ_J. The complex landscape of an N-particle packing in d dimensions is the $Nd-1$ dimensional potential energy surface in the Nd space of translational degrees of freedom associated with the positions of the particles. Typically, in the thermodynamic limit a jammed system is only marginally stable to perturbations (18–25); that is, an infinitesimal perturbation suffices to rearrange the packing, pushing the system into a new local energy minimum. Because material stability is a key property governing the response of a material under shear and deformation, such as the transition from ductile to brittle behavior (26), producing jammed packings with high mechanical stability has been an active area of interest (13–17, 27–31).

Some of these works (15, 27) have started to develop organizing principles to explain how free-then-freeze optimization, specifically focused on changing particle radii, can drive high stability in jammed packings. In particular, the swap Monte Carlo protocol allows changes in the radii of the particles but only to values that are drawn from a fixed set. The algorithm that we introduce here can be generalized to any set of degrees of freedom in a variety of optimization and annealing processes. It therefore should be a powerful tool in computational studies of soft materials. In addition, a broader understanding of which variables are important to constrain, and why, has remained elusive. Here we introduce a set of global free-then-freeze protocols and apply them to jammed packings. We contrast how involving two different sets of learning degrees of freedom affects material stability. We find that not all degrees of freedom are equally useful for evolving a desired function and show that this can be explained by an analysis of how the constraints enter into the dynamical equations.

Manipulating learning degrees of freedom in this transient way accesses local minima that not only have low energy but also have high-energy barriers preventing escape. By understanding which variables alter stability the most, we can better understand the factors that control the effectiveness of specific preparation protocols, potentially opening up new avenues for the rational design and manipulation of materials.

Protocol Details. We study packings of spheres in three dimensions (3D). Particles, labeled by i and j, interact via finite-range, repulsive harmonic potentials:

$$U=\frac{1}{2}\sum_{i,j}\epsilon_{ij}\left(1-\frac{|\mathbf{X}_i-\mathbf{X}_j|}{R_i+R_j}\right)^2\Theta\left(1-\frac{|\mathbf{X}_i-\mathbf{X}_j|}{R_i+R_j}\right), \quad [1]$$

where $\mathbf{X}_i$ and R_i are the position and radius of particle i, and $\epsilon_{ij}=\frac{K_iK_j}{K_i+K_j}$ is the interaction stiffness between particles i and j. As is standard, the individual stiffnesses of particles K_i and K_j are added like springs in series to produce the effective interaction between them. The Heaviside step function allows only positive overlaps between particles to contribute.

We generate jammed packings by randomly and uniformly distributing N soft particles at a given packing fraction, ϕ (which is the sum of all particle volumes divided by the volume of the box), in a cubic box with periodic boundary conditions. The initial state will in general not be at a local energy minimum due to the overlap of particles subject to the energy function given by Eq. **1**. We minimize the energy with respect to the degrees of freedom to bring the system to a jammed state at mechanical equilibrium (32, 33). In a conventional packing at fixed volume, the physical degrees of freedom–particle positions–are the only degrees of freedom with respect to which the energy is minimized. Here we consider two additional sets of learning degrees of freedom, namely, the particle radii, $\{R_i\}$, and stiffnesses, $\{K_i\}$. We minimize the energy with respect to the degrees of freedom using pyCUDAPacking (19, 34), incorporating a quad-precision graphics processing unit implementation of the Fast Inertial Relaxation Engine (FIRE). FIRE is a molecular dynamics–based minimization algorithm that relies on inertia and uses the gradient of the energy to bring a system of particles to a local energy minimum (35).

With either R_i or K_i as learning degrees of freedom, there are trivial zero-energy minima to which the system can escape. For example, a sufficient number of the radii can shrink in order to remove all overlaps, or the stiffness cost of overlaps can adjust to zero. To avoid such trivial states, we constrain some of the moments, m, of the distributions of the newly introduced variables so that $\Phi_{\chi,m}\equiv\sum_i\chi_i^m$ are fixed, where χ_i can be either R_i or K_i. For $\chi_i=R_i$, fixing the packing fraction $\phi\propto\Phi_{R,3}=\sum_i R_i^3$ is not sufficient to prevent some radii from shrinking to zero. By choosing constraints with both negative and positive powers of χ_i, namely, $m=\{-3,-2,-1,1,2,3,6\}$, we are able to minimize all of the systems presented in this paper without appreciably altering the radius or stiffness distributions (Fig. 1). Note that the packing fraction is fixed since we keep the third moment of the radii fixed. The set of constraints used here is not special, and one can produce similar results with other $\{m\}$ similarly including both positive and negative powers of χ_i. One can also introduce a larger number of constraints to keep the initial distributions fixed. In the case of radii, this would lead to results that are similar to the outcome of the swap Monte Carlo algorithm, but the minimization becomes subsequently slower without producing appreciably different results. Here we report data for 3D packings with log-normal distributions of initial and final polydispersity of 20% in $\{R_i\}$ or $\{K_i\}$ (except in Fig. 1 where multiple polydispersities are reported). Note that this protocol is not applicable to monodisperse packings since it is not possible to start with a monodisperse packing, update the radii, and still retain a monodisperse packing.

To impose the constraints during minimization, we restrict changes in the newly introduced variables to subspaces in which all constraints are satisfied. The subspace of allowed values is the space spanned by vectors $\nabla_\chi(\sum_i\chi_i^m)$. We identify the unit vectors, $\hat{\mathbf{n}}_{\chi,m}$ that form a complete orthonormal basis for this subspace and project out force components perpendicular to the subspace:

$$\mathbf{f}_{\chi,\{m\}}=\mathbf{f}_\chi-\sum_m(\mathbf{f}_\chi\cdot\hat{\mathbf{n}}_{\chi,m})\,\hat{\mathbf{n}}_{\chi,m}. \quad [2]$$

These forces are used in the FIRE minimizer to update radii and stiffnesses; particle positions are updated without any constraints.

Measuring Stability. We measure stability in three ways (Fig. 2). Fig. 2 *A* and *B* present the increase in pressure, δP, needed to destabilize the system (see *SI Appendix* for details). Fig. 2*A* shows that radius-minimized packings (red) require a much larger change in pressure to become unstable compared to ordinary packings with the same radius distribution. Note that $\delta P\to$ constant at low pressure for the radius-minimized packings. This is in contrast to $\delta P\to 0$ as $P\to 0$ for ordinary packings, reflecting marginal stability at the jamming transition. Fig. 2*B* shows that the pressure change required to destabilize a stiffness-minimized packing (blue) is also larger than that of a conventionally prepared packing with the same distribution of particle stiffnesses (black) but vanishes as $P\to 0$. This result shows that the stiffness degrees

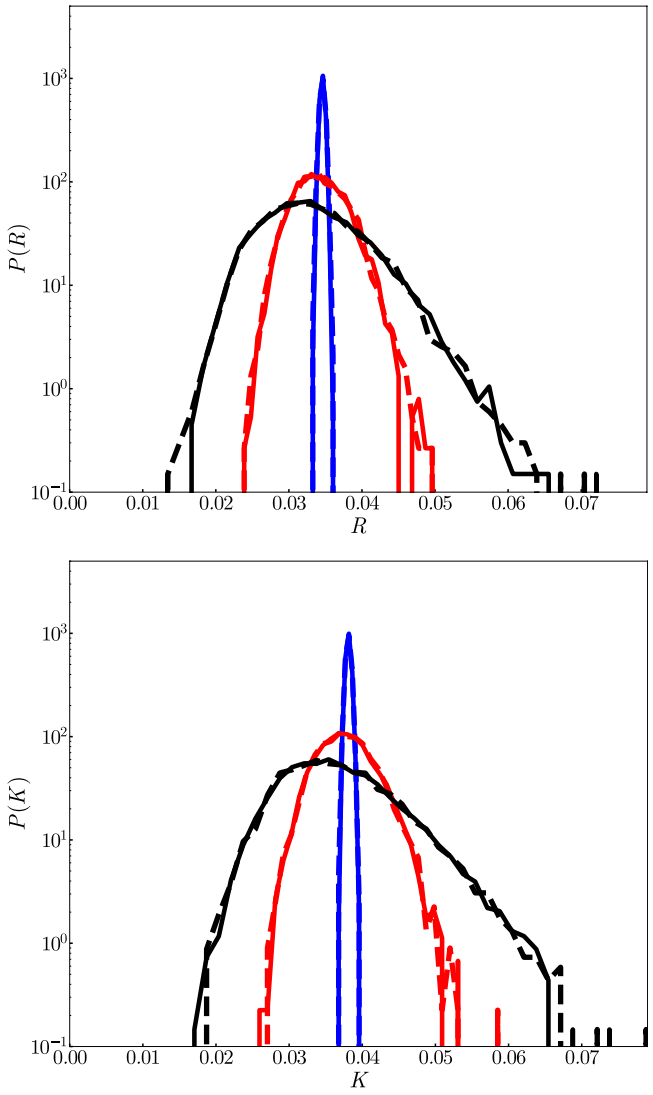

Fig. 1. Distributions of (*Top*) radii and (*Bottom*) stiffnesses before (solid) and after (dashed) minimization in 3D packings. The different distributions have different fractional widths about their average value: 1% (blue), 10% (red), and 20% (black). Each packing has $N = 4096$ particles and is prepared at a pressure of $p = 10^{-2}$.

of freedom become less effective in increasing stability as the pressure decreases. Fig. 2 *A* and *B*, *Insets*, show that for radius- and stiffness-minimized packings, δP is independent of system size for large N at $P = 10^{-4}$. This suggests that in the thermodynamic limit, one can use this protocol to create jammed packings that are fully stable and therefore energetically rigid (36), not marginally stable like ordinary jammed packings.

Fig. 2 *C* and *D* show the density of vibrational modes $\mathcal{D}(\omega)$. Prior work has shown that for jammed packings, the average energy barriers associated with vibrational modes increase monotonically with mode frequency, ω (37). This suggests that when the low-frequency tail of $\mathcal{D}(\omega)$ shifts to higher values, the system becomes more stable because the energy barrier heights increase, preventing the system from easily moving from one local minimum to another.

Fig. 2*C* shows that when radius degrees of freedom are allowed to vary, the low-ω modes (magenta data) extend to much lower frequencies than conventionally prepared packings (black data). These low-frequency modes are coupled to positional degrees of freedom and create a plateau in the density of states. Once the radius degrees of freedom are frozen at their equilibrium values (after the minimization has taken place), the shape of $\mathcal{D}(\omega)$ changes dramatically (red data), shifting the low end of the plateau to much higher frequency.

In contrast, when stiffness degrees of freedom are allowed, as shown in Fig. 2*D* (cyan data), a band of very low-frequency modes appears. These modes are uncoupled to the position variables, which are responsible for the band of modes at higher frequencies that is essentially the same as for ordinary jammed packings (black). Between these two sets of modes there is a pronounced band gap. When the stiffness degrees of freedom are frozen after minimization (blue), however, the low-frequency band disappears, leaving only a density of states that is very similar to that of a conventionally prepared packing (black) with the same stiffness distribution.

Finally, Fig. 2 *E* and *F* show measurements of the crossover frequency ω^*, marking the low-frequency end of the plateau in the density of vibrational states, for the radius (red) and stiffness-minimized packings (blue), respectively. In the conventionally prepared jammed packings (black), $\omega^* \propto P^{1/2}$ (38). As shown by the red data in Fig. 2*E*, ω^* approaches a constant as pressure P is lowered for the radius-minimized packings. By contrast, for the stiffness-minimized packings (blue), $\omega^* \propto P^{1/2}$ as in conventional packings, albeit with a slightly higher prefactor. This behavior again points to a clear distinction between the radius and stiffness degrees of freedom. The radius-minimized packings behave like conventional packings far above the jamming threshold (at much higher pressure), while stiffness-minimized packings are similar to conventional packings at the same pressure. Fig. 2 *E* and *F*, *Insets*, show that $\omega^* \to$ constant at large N at $P = 10^{-4}$, suggesting it is nonzero as $N \to \infty$.

Different Types of Learning Degrees of Freedom. Fig. 2 shows that adding and then freezing either the radius or stiffness degrees of freedom leads to enhanced stability in jammed packings. However, the stability gained from the radii is qualitatively different from that gained from stiffnesses. This distinction stems from a fundamental difference in how radius and stiffness degrees of freedom affect the onset of rigidity in jammed systems.

This difference is shown in Fig. 3, where we plot pressure, P, vs. the number of contacts per particle, Z, in radius- and stiffness-minimized packings as well as conventional ones. Introducing radii as learning degrees of freedom shifts the critical point from $Z_c = 2d$ to a much higher value $Z_c = 2(d+1)$ (ignoring terms of order $1/N$), which lies deep within the stable regime (22). By contrast, stiffness degrees of freedom do not alter the onset of rigidity. Particle stiffnesses become irrelevant to the mechanics of the system as $P \to 0$ when the particles are just in contact and do not overlap. Fig. 3, *Inset*, which shows the scaling of pressure with respect to the number of excess contacts per particle, $(Z - Z_c)$, indicates that the scaling behaviors of the jamming transition do not change under the free-then-freeze protocol.

This can be understood from the role that radius and stiffness variables play in the rigidity (compatibility) matrix, $\mathbf{C}$. This is the matrix of coefficients in the linear equations relating changes in the degrees of freedom to changes in the constraints. Here most of the constraints punish overlaps between particles $h_{ij} = 1 - \frac{|\mathbf{X}_i - \mathbf{X}_j|}{R_i + R_j}$, meaning that $C_{ij} = \partial h_{ij}/\partial \chi_i$, where χ_i can be X_i, R_i, or K_i. Maxwell's constraint count (39) is then derived using the rank-nullity theorem [for a linear transformation, T, in an n dimensional space, rank(T) + nullity $(T) = n$] on the rigidity matrix $\mathbf{C}$ and its transpose $\mathbf{C}^T$. Since the stiffnesses do not affect which particles overlap, they do not appear as independent columns in the rigidity matrix. This means that stiffnesses do

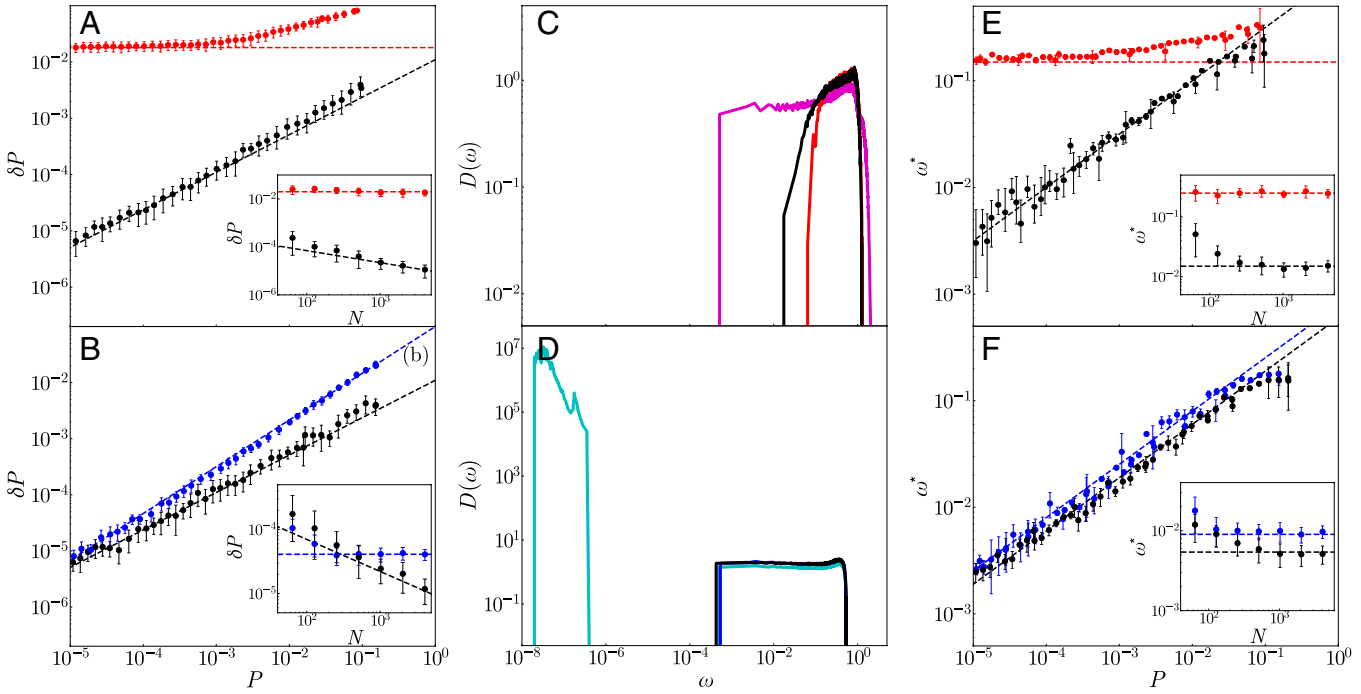

Fig. 2. The increase in pressure, δP, required to make a packing unstable for (*A*) radius- (red) and (*B*) stiffness-minimized (blue) packings as well as conventional packings (black) with the same distributions of radii and stiffness. Black dashed lines show a power law $\delta P \propto P^{2/3}$, the red dashed line in *A* is constant (zero slope), and the blue dashed line in *B* shows $\delta P \propto P^{5/6}$. (*Insets*) δP versus system size N at $P = 10^{-4}$. Black dashed lines indicate $\delta P \propto P^{-1/3}$. Density of states, $\mathcal{D}(\omega)$ versus ω, for (*C*) radius and (*D*) stiffness-minimized packings near jamming transition at $\phi \simeq 0.70$ and $\phi \simeq 0.64$, respectively. The magenta (*C*) and cyan (*D*) curves show $\mathcal{D}(\omega)$ when radii and stiffnesses are considered as degrees of freedom, while the red (*C*) and blue (*D*) curves show $\mathcal{D}(\omega)$ once radii/stiffnesses are frozen at their equilibrium values after minimization. The black curves in both plots show the density of states for conventional packings with the same radii and stiffness distributions. ω^* versus pressure P for (*E*) radius (red) and (*F*) stiffness-minimized (blue) packings. The black data in both panels represent conventional packings. Black dashed lines in both plots are a power law of $\omega^* \propto P^{1/2}$. (*Insets*) Ensemble averaged ω^* versus system size, N, for packings at pressure $P = 10^{-4}$. The lines have zero slope. Data points in the main plots are averaged over 20 samples each with $N = 1024$ particles.

not change the rank of the rigidity matrix and therefore cannot change the number of contacts at the transition point, given by the Maxwell's count (see *SI Appendix* for further details).

Discussion

In this paper, we have shown that introducing particle sizes and stiffnesses as transient learning degrees of freedom into the quenching process of jammed packings allows the creation of particularly stable packings with deep minima and high-energy barriers against rearrangements. However, not every degree of freedom is equally effective in this process; because they do not couple to the jamming transition, the stiffnesses do not affect the stability as profoundly as the particle radii do. We also note that while introducing N extra degrees of freedom (one per particle), we needed to impose only a few global constraints on the moments of the radius (or stiffness) distributions to ensure that the minimization did not flow to a different fixed point where one particle grew (or became stiffer) at the expense of all the others. For the system sizes considered, $N \leq 4096$, we imposed seven constraints. For smaller systems, we needed to impose fewer constraints to obtain similar quantitative results. It is likely that as N increases, more constraints are needed. It would be interesting to study the importance and number of constraints on the distributions that are needed in the asymptotically large-N limit.

We note that our work builds on a previously introduced free-then-freeze protocol involving "breathing" particles for jammed packings (15, 27). As in our work, the learning degrees of freedom are the particle radii. However, in the case of breathing particles, each of the N radii, or learning degrees of freedom, is subject to a constraint. In our case, we place the minimal number of constraints, far fewer than N, on moments of the learning degrees of freedom distributions. This allows us to reach far more stable local minima, making our free-then-freeze protocol more effective.

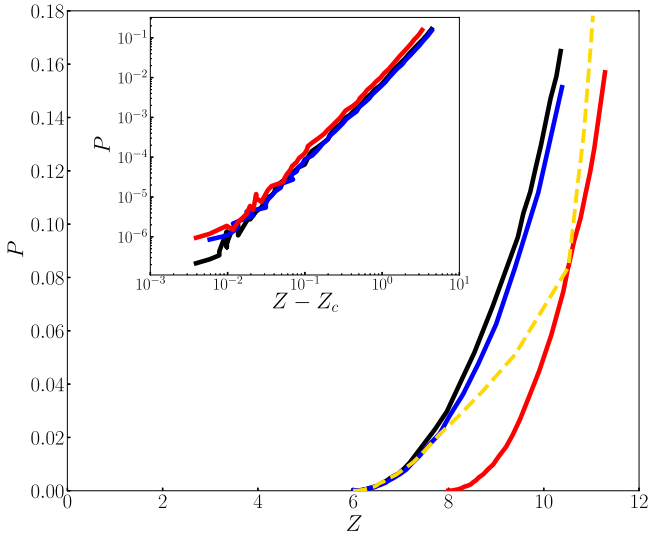

Fig. 3. Pressure, P, versus coordination, Z, for radius- (red) and stiffness- (blue) minimized packings in comparison to conventional (black) packings. The dashed yellow line shows the change in P and Z when a radius-minimized packing is pushed to higher or lower pressures using positions as the only allowed degrees of freedom. (*Inset*) The pressure against distance from critical point in logarithmic scale. For the red curve, the critical point occurs at $Z_c = 2(d+1)$, while for the blue and black curves, the critical point occurs at $Z_c = 2d$.

The introduction of transient learning degrees of freedom provides a unifying conceptual framework for the evolution of a variety of systems in complex energy or fitness landscapes. Appropriate training protocols can lead the disordered materials to occupy desired metastable states with useful properties (5, 8, 10, 12, 40–42). These ideas can be generalized to processing in experimental systems where the learning degrees of freedom can be ordinary translational ones. For example, with the right deposition protocol, vapor-deposited glasses have been created that are exceedingly stable (43–45). In the context of transient learning degrees of freedom, the particles at a free surface have more degrees of freedom than those within the bulk. These variables can be considered learning degrees of freedom that freeze as more particles are deposited and the particles become buried in the bulk.

As another example, one can interpret aging in supercooled liquids and glasses in terms of transient learning degrees of freedom. Upon aging, the relaxation times increase dramatically so that these pathways are inaccessible at short times. The relaxation itself produces a separation of time scales (46, 47). The system, as it ages, limits the possibility of using the degrees of freedom (i.e., the relaxation pathways) so that they can also be considered to be transient learning degrees of freedom. This raises the possibility of using them as learning degrees of freedom to introduce desired properties.

The concept of additional transient learning degrees of freedom is useful for thinking about many different protocols that have been used to create novel function in systems that exist in rugged landscapes. While in some cases this leads only to a reinterpretation of what was already known, it serves the important purpose of allowing one to think about what kinds of new and different variables would be useful as a means to manipulate matter in new ways. A particularly interesting possibility to explore would be to introduce particle shapes as learning degrees of freedom. Because shape couples strongly to the Maxwell's count at the jamming transition, it could therefore lead to a large increase in stability. The degrees of freedom studied in this paper can also be used to train for other functions as distinct from increased stability. For example, one could consider training for a particular force network or for creating an allosteric interaction between distant particles. In this case, it is not clear which newly introduced set of variables, radii or stiffnesses, would be better at training for this function. This question can be generalized to any desired function and any set of transient learning degrees of freedom. We envision mapping the free-then-freeze protocol onto a supervised learning framework that uses explainability tools to identify the best set of degrees of freedom for any function. Similarly, in materials like origami (48), fiber networks, or biological tissues (36, 49) that rigidify by higher-order terms beyond constraint counting, we speculate that it may be fruitful to examine how different degrees of freedom affect those higher-order constraints.

Data Availability. All study data are included in the article and/or *SI Appendix*.

ACKNOWLEDGMENTS. We thank R. Cameron Dennis for assistance with the constrained minimization algorithms. This work is supported by the Simons Foundation for the collaboration Cracking the Glass Problem via awards 454939 (E.I.C.), 454945 (A.J.L.), 348126 (V.F.H. and S.R.N.), and 454947 (M.L.M.) and Investigator Awards 327939 (A.J.L.) and 446222 (M.L.M.), as well as by the US Department of Energy, Office of Science, Basic Energy Sciences, under Grant DE-SC0020972 (for studying implications of training in biological systems; S.R.N.). The comparison with experimental systems was partially supported by the University of Chicago Materials Research Science and Engineering Center funded by the NSF under award DMR-2011854.

1. F. Krzakala, J. Kurchan, Landscape analysis of constraint satisfaction problems. *Phys. Rev. E Stat. Nonlin. Soft Matter Phys.* **76**, 021122 (2007).
2. M. Mézard, T. Mora, Constraint satisfaction problems and neural networks: A statistical physics perspective. *J. Physiol. Paris* **103**, 107–113 (2009).
3. A. Altieri, S. Franz, Constraint satisfaction mechanisms for marginal stability and criticality in large ecosystems. *Phys. Rev. E* **99**, 010401 (2019).
4. P. Mehta, W. Cui, C. H. Wang, R. Marsland, III, Constrained optimization as ecological dynamics with applications to random quadratic programming in high dimensions. *Phys. Rev. E* **99**, 052111 (2019).
5. C. P. Goodrich, A. J. Liu, S. R. Nagel, The principle of independent bond-level response: Tuning by pruning to exploit disorder for global behavior. *Phys. Rev. Lett.* **114**, 225501 (2015).
6. V. F. Hagh, M. Thorpe, Disordered auxetic networks with no reentrant polygons. *Phys. Rev. B* **98**, 100101 (2018).
7. V. F Hagh, E. I. Corwin, K. Stephenson, M. F. Thorpe, A broader view on jamming: From spring networks to circle packings. *Soft Matter* **15**, 3076–3084 (2019).
8. D. Hexner, A. J. Liu, S. R. Nagel, Linking microscopic and macroscopic response in disordered solids. *Phys. Rev. E* **97**, 063001 (2018).
9. D. Hexner, A. J. Liu, S. R. Nagel, Role of local response in manipulating the elastic properties of disordered solids by bond removal. *Soft Matter* **14**, 312–318 (2018).
10. N. Pashine, D. Hexner, A. J. Liu, S. R. Nagel, Directed aging, memory, and nature's greed. *Sci. Adv.* **5**, eaax4215 (2019).
11. D. Hexner, N. Pashine, A. J. Liu, S. R. Nagel, Effect of directed aging on nonlinear elasticity and memory formation in a material. *Phys. Rev. Res.* **2**, 043231 (2020).
12. D. Hexner, A. J. Liu, S. R. Nagel, Periodic training of creeping solids. *Proc. Natl. Acad. Sci. U.S.A.* **117**, 31690–31695 (2020).
13. A. Ninarello, L. Berthier, D. Coslovich, Models and algorithms for the next generation of glass transition studies. *Phys. Rev. X* **7**, 021039 (2017).
14. H. Ikeda, F. Zamponi, A. Ikeda, Mean field theory of the swap Monte Carlo algorithm. *J. Chem. Phys.* **147**, 234506 (2017).
15. C. Brito, E. Lerner, M. Wyart, Theory for swap acceleration near the glass and jamming transitions for continuously polydisperse particles. *Phys. Rev. X* **8**, 031050 (2018).
16. L. Berthier, E. Flenner, C. J. Fullerton, C. Scalliet, M. Singh, Efficient swap algorithms for molecular dynamics simulations of equilibrium supercooled liquids. *J. Stat. Mech. Theory Exp* **2019**, 064004 (2019).
17. A. D. S. Parmar, B. Guiselin, L. Berthier, Stable glassy configurations of the Kob-Andersen model using swap Monte Carlo. *J. Chem. Phys.* **153**, 134505 (2020).
18. R. Connelly, W. Whiteley, Second-order rigidity and prestress stability for tensegrity frameworks. *SIAM J. Discret. Math.* **9**, 453–491 (1996).
19. P. Charbonneau, E. I. Corwin, G. Parisi, F. Zamponi, Universal microstructure and mechanical stability of jammed packings. *Phys. Rev. Lett.* **109**, 205501 (2012).
20. C. P. Goodrich, W. G. Ellenbroek, A. J. Liu, Stability of jammed packings. I: The rigidity length scale. *Soft Matter* **9**, 10993–10999 (2013).
21. C. P. Goodrich *et al.*, Jamming in finite systems: Stability, anisotropy, fluctuations, and scaling. *Phys. Rev. E Stat. Nonlin. Soft Matter Phys.* **90**, 022138 (2014).
22. E. DeGiuli, A. Laversanne-Finot, G. Düring, E. Lerner, M. Wyart, Effects of coordination and pressure on sound attenuation, boson peak and elasticity in amorphous solids. *Soft Matter* **10**, 5628–5644 (2014).
23. R. Connelly, S. Guest, *Frameworks, Tensegrities and Symmetry: Understanding Stable Structures* (College of Arts and Sciences, Cornell University, 2015).
24. M. Müller, M. Wyart, Marginal stability in structural, spin, and electron glasses. *Annu. Rev. Condens. Matter Phys.* **6**, 177–200 (2015).
25. N. Xu, A. J. Liu, S. R. Nagel, Instabilities of jammed packings of frictionless spheres under load. *Phys. Rev. Lett.* **119**, 215502 (2017).
26. W. T. Yeh, M. Ozawa, K. Miyazaki, T. Kawasaki, L. Berthier, Glass stability changes the nature of yielding under oscillatory shear. *Phys. Rev. Lett.* **124**, 225502 (2020).
27. C. Brito, H. Ikeda, P. Urbani, M. Wyart, F. Zamponi, Universality of jamming of nonspherical particles. *Proc. Natl. Acad. Sci. U.S.A.* **115**, 11736–11741 (2018).
28. G. Kapteijns, W. Ji, C. Brito, M. Wyart, E. Lerner, Fast generation of ultrastable computer glasses by minimization of an augmented potential energy. *Phys. Rev. E* **99**, 012106 (2019).
29. H. Ikeda, P. Urbani, F. Zamponi, Mean field theory of jamming of nonspherical particles. *J. Phys. A Math. Theor.* **52**, 344001 (2019).
30. T. Yanagishima, J. Russo, R. P. A. Dullens, H. Tanaka, Towards glasses with permanent stability. *Phys. Rev. Lett.* **127**, 215501 (2021).
31. H. Ikeda, C. Brito, M. Wyart, Infinitesimal asphericity changes the universality of the jamming transition. *J. Stat. Mech. Theory Exp.* **2020**, 033302 (2020).
32. D. J. Durian, Foam mechanics at the bubble scale. *Phys. Rev. Lett.* **75**, 4780–4783 (1995).
33. C. S. O'Hern, L. E. Silbert, A. J. Liu, S. R. Nagel, Jamming at zero temperature and zero applied stress: The epitome of disorder. *Phys. Rev. E Stat. Nonlin. Soft Matter Phys.* **68**, 011306 (2003).
34. P. K. Morse, E. I. Corwin, Geometric signatures of jamming in the mechanical vacuum. *Phys. Rev. Lett.* **112**, 115701 (2014).
35. E. Bitzek, P. Koskinen, F. Gähler, M. Moseler, P. Gumbsch, Structural relaxation made simple. *Phys. Rev. Lett.* **97**, 170201 (2006).
36. O. K. Damavandi, V. F. Hagh, C. D. Santangelo, M. L. Manning, Energetic rigidity. I. A unifying theory of mechanical stability. *Phys. Rev. E* **105**, 025003 (2022).
37. N. Xu, V. Vitelli, A. J. Liu, S. R. Nagel, Anharmonic and quasi-localized vibrations in jammed solids–Modes for mechanical failure. *Europhys. Lett.* **90**, 56001 (2010).
38. L. E. Silbert, A. J. Liu, S. R. Nagel, Vibrations and diverging length scales near the unjamming transition. *Phys. Rev. Lett.* **95**, 098301 (2005).
39. J. C. Maxwell, On the calculation of the equilibrium and stiffness of frames. *Lond. Edinb. Dublin Philos. Mag. J. Sci.* **27**, 294–299 (1864).
40. J. W. Rocks *et al.*, Designing allostery-inspired response in mechanical networks. *Proc. Natl. Acad. Sci. U.S.A.* **114**, 2520–2525 (2017).
41. J. W. Rocks, H. Ronellenfitsch, A. J. Liu, S. R. Nagel, E. Katifori, Limits of multifunctionality in tunable networks. *Proc. Natl. Acad. Sci. U.S.A.* **116**, 2506–2511 (2019).

42. M. Stern, D. Hexner, J. W. Rocks, A. J. Liu, Supervised learning in physical networks: From machine learning to learning machines. *Phys. Rev. X* **11**, 021045 (2021).
43. S. F. Swallen *et al.*, Organic glasses with exceptional thermodynamic and kinetic stability. *Science* **315**, 353–356 (2007).
44. K. L. Kearns *et al.*, Hiking down the energy landscape: Progress toward the Kauzmann temperature via vapor deposition. *J. Phys. Chem. B* **112**, 4934–4942 (2008).
45. M. D. Ediger, Perspective: Highly stable vapor-deposited glasses. *J. Chem. Phys.* **147**, 210901 (2017).
46. M. D. Ediger, C. A. Angell, S. R. Nagel, Supercooled liquids and glasses. *J. Phys. Chem.* **100**, 13200–13212 (1996).
47. L. Berthier, Time and length scales in supercooled liquids. *Phys. Rev. E Stat. Nonlin. Soft Matter Phys.* **69**, 020201 (2004).
48. B. G.-g. Chen, C. D. Santangelo, Branches of triangulated origami near the unfolded state. *Phys. Rev. X* **8**, 011034 (2018).
49. O. K. Damavandi, V. F. Hagh, C. D. Santangelo, M. L. Manning, Energetic rigidity. II. Applications in examples of biological and underconstrained materials. *Phys. Rev. E* **105**, 025004 (2022).